Successful Reproduction Requires the Function of Arabidopsis YELLOW STRIPE-LIKE1 and YELLOW STRIPE-LIKE3 Metal-Nicotianamine Transporters in Both Vegetative and Reproductive Structures[1][W][OA]

Heng-Hsuan Chu, Jeff Chiecko, Tracy Punshon, Antonio Lanzirotti, Brett Lahner, David E. Salt, and Elsbeth L. Walker*

Plant Biology Graduate Program (H.-H.C., J.C.) and Department of Biology (E.L.W.), University of Massachusetts, Amherst, Massachusetts 01003; Department of Biological Sciences, Dartmouth College, Hanover, New Hampshire 03755 (T.P.); Consortium for Advanced Radiation Sources, University of Chicago, Chicago, Illinois 60637 (A.L.); and Center for Plant Environmental Stress Physiology, Purdue University, West Lafayette, Indiana 47907 (B.L., D.E.S.)

Several members of the Yellow Stripe-Like (YSL) family of proteins are transporters of metals that are bound to the metal chelator nicotianamine or the related set of mugineic acid family chelators known as phytosiderophores. Here, we examine the physiological functions of three closely related Arabidopsis (*Arabidopsis thaliana*) YSL family members, AtYSL1, AtYSL2, and AtYSL3, to elucidate their role(s) in the allocation of metals into various organs of Arabidopsis. We show that AtYSL3 and AtYSL1 are localized to the plasma membrane and function as iron transporters in yeast functional complementation assays. By using inflorescence grafting, we show that AtYSL1 and AtYSL3 have dual roles in reproduction: their activity in the leaves is required for normal fertility and normal seed development, while activity in the inflorescences themselves is required for proper loading of metals into the seeds. We further demonstrate that the AtYSL1 and AtYSL2 proteins, when expressed from the *AtYSL3* promoter, can only partially rescue the phenotypes of a *ysl1ysl3* double mutant, suggesting that although these three YSL transporters are closely related and have similar patterns of expression, they have distinct activities in planta. In particular, neither *AtYSL1* nor *AtYSL2* is able to functionally complement the reproductive defects exhibited by *ysl1ysl3* double mutant plants.

The transition metals iron (Fe), copper (Cu), and zinc (Zn) are among the most important and most problematic of all the micronutrients used by plants. The importance of these metals stems from their roles as essential cofactors for cellular redox reactions involved in photosynthesis, respiration, and many other reactions. The problematic nature of these metals stems from the same distinct chemical properties that make them so valuable to living systems. These metals, particularly Cu and Fe, are highly reactive and, if overaccumulated, can cause cellular redox damage. Fe presents an additional problem for plants, because it is also only sparingly soluble in aqueous solution and thus is typically not "bioavailable" in soil (Guerinot and Yi, 1994). As a response to these key properties, plants have evolved multifaceted systems to control metal uptake by the root, translocation through the plant body, storage within tissues, and remobilization during reproduction and times of nutrient stress.

The nonproteinogenic amino acid nicotianamine (NA) is a strong complexor of various transition metals, particularly Fe(II) (Anderegg and Ripperger, 1989) and Fe(III) (von Wiren et al., 1999), as well as Cu (II), Ni(II), Co(II), Mn(II), and Zn(II) (Anderegg and Ripperger, 1989). NA is present in shoots and roots at concentrations ranging between 20 and 500 nM g^{-1}

[1] This work was supported by the National Science Foundation (grant nos. MCB0114748 and IOS0847687 to E.L.W. and IOB0419695 to D.E.S.), the U.S. Department of Agriculture National Research Initiative Competitive Grants Program (grant no. 2005–01072 to E.L.W.), the Indiana 21st Century Research and Technology Fund (grant no. 912010479 to D.E.S.), and the National Institute of Environmental Health Sciences, Superfund Basic Research Program (grant no. P42 ES007373–14 to T.P.). A portion of this work was performed at Beamline X26A, National Synchrotron Light Source, Brookhaven National Laboratory. X26A is supported by the Department of Energy-Geosciences (grant no. DE–FG02–92ER14244 to the University of Chicago Consortium for Advanced Radiation Sources) and Department of Energy-Office of Biological and Environmental Research, Environmental Remediation Sciences Division (grant no. DE–FC09–96–SR18546 to the University of Kentucky). Use of the National Synchrotron Light Source was supported by the Department of Energy (contract no. DE–AC02–98CH10886).

* Corresponding author; e-mail ewalker@bio.umass.edu.

The author responsible for distribution of materials integral to the findings presented in this article in accordance with the policy described in the Instructions for Authors (www.plantphysiol.org) is: Elsbeth L. Walker (ewalker@bio.umass.edu).

[W] The online version of this article contains Web-only data.

[OA] Open Access articles can be viewed online without a subscription.

www.plantphysiol.org/cgi/doi/10.1104/pp.110.159103

fresh weight (Stephan et al., 1990) and is present in both xylem (approximately 20 μM [Pich and Scholz, 1996]) and phloem (approximately 130 μM [Schmidke and Stephan, 1995]), suggesting that it is a major complexor of metals throughout the plant. Much of what we know about NA function in plants comes from studies of a mutant of tomato (*Solanum lycopersicum*) called *chloronerva*, in which the single gene encoding NA synthase is disrupted (Herbik et al., 1999; Higuchi et al., 1999; Ling et al., 1999). The *chloronerva* phenotype is complex. Plants exhibit interveinal chlorosis in young leaves and constitutively activate their root Fe uptake systems, indicating that they have inadequate Fe. However, mature leaves of *chloronerva* mutants contain excess Fe, implying that the Fe that is present is not being properly localized in the absence of NA. These *chloronerva* plants also have severe defects in translocation of Cu in the xylem, indicating a clear role for NA in Cu transport. The plants are sterile, indicating that NA is important during plant reproduction. Complementing these classical studies on *chloronerva*, Takahashi et al. (2003) have developed tobacco (*Nicotiana tabacum*) plants that heterologously express a barley (*Hordeum vulgare*) gene encoding the enzyme NA aminotransferase, which converts NA into a nonfunctional intermediate. Recently, the phenotype of quadruple *NA synthase* mutants was described in Arabidopsis (*Arabidopsis thaliana*; Klatte et al., 2009). In both studies, the plants exhibited many of the defects caused by the *chloronerva* mutation, including chlorosis and an array of reproductive abnormalities.

Several members of the well-conserved Yellow Stripe-Like (YSL) family of proteins function as metal-NA transporters (DiDonato et al., 2004; Koike et al., 2004; Roberts et al., 2004; Schaaf et al., 2004; Murata et al., 2006; Gendre et al., 2007). The founding member of the YSL family, maize (*Zea mays*) Yellow Stripe1 (ZmYS1), is the primary means by which roots of grasses take up Fe from the soil. The grasses, a group that includes most of the world's staple grains (e.g. rice [*Oryza sativa*], wheat [*Triticum aestivum*], and maize), use a chelation strategy for primary Fe uptake. In response to Fe starvation, grasses secrete phytosiderophores (PS): derivatives of the mugineic acid family that are structurally similar to NA and that form stable Fe(III) chelates in soil (Tagaki et al., 1984). This accomplishes solubilization of the otherwise nearly insoluble soil Fe. The YS1 protein, located at the root surface, then moves the Fe(III)-PS complexes from the rhizosphere into root cells (Romheld and Marchner, 1986; Curie et al., 2001; Roberts et al., 2004)

Arabidopsis has eight *YSL* genes. Three of these (*AtYSL1*, At4g24120; *AtYSL2*, At5g24380; and *AtYSL3*, At5g53550) are expressed strongly in the xylem parenchyma of leaves and are down-regulated during Fe deficiency (DiDonato et al., 2004; Waters et al., 2006). We have previously shown that double mutant plants with lesions in both *AtYSL1* and *AtYSL3* display strong interveinal chlorosis. We have hypothesized that the function of these YSL transporters in vegetative tissues is to take up Fe that arrives in leaves via the xylem (Waters et al., 2006). All of the defects displayed by *ysl1ysl3* double mutants can be alleviated if excess Fe is applied to the soil, demonstrating that these growth defects are caused primarily by a lack of Fe. Intriguingly, although Fe deficiency appears to be the basis of the double mutant phenotype, the concentrations of several metals are specifically altered in the double mutants (Waters et al., 2006). *AtYSL1* single mutant plants have subtle phenotypes, the most striking of which is a decrease in both NA and Fe in seeds (Le Jean et al., 2005). Interestingly, leaves of these mutants contain excess NA, while Fe levels are normal. These observations are consistent with the more obvious and extensive phenotypes exhibited by the *ysl1ysl3* double mutant and highlight the idea that AtYSL proteins affect the homeostasis of both Fe and NA.

In addition to the vegetative defects mentioned above, the *ysl1ysl3* double mutant has multiple defects in reproduction. Double mutant flowers produce few functional pollen grains and thus exhibit greatly reduced fertility. Many of the seeds that these plants do manage to produce are small and contain embryos arrested at various immature stages, which often fail to germinate. These fertility defects can be reversed by application of Fe-ethylenediamine-*N*,*N*′-bis(2-hydroxyphenylacetic acid) solution to the soil, again demonstrating that these growth defects are caused by a lack of Fe (Waters et al., 2006). Expression of *YSL1* and *YSL3* is very limited in flowers and developing siliques; furthermore, the patterns of expression of *YSL1* and *YSL3* are distinct and largely nonoverlapping in these structures. However, expression of *AtYSL1* and *AtYSL3* increases markedly during leaf senescence, a period in which many minerals are remobilized from leaves, presumably for delivery into developing seeds (Himelblau and Amasino, 2001). This model is in good agreement with the accepted model for nutrient loading into seeds proposed originally by Hocking and Pate (1977, 1978), which suggests that metals mobilized from vegetative structures account for 20% to 30% of the content in seeds. Direct measurements of metals in senescing and younger leaves demonstrated that double mutants failed to mobilize Zn and Cu from leaves. Seeds produced by the double mutant plants contained reduced levels of Zn and Cu, the same metals that failed to be mobilized out of the leaves (Waters et al., 2006). This led us to propose a model in which the activity of AtYSL1 and AtYSL3 in leaves was required for correct localization of metals into the seeds. However, seeds also had low Fe levels, even though Fe appeared to be mobilized normally from leaves of the double mutants.

Here, we further investigate the role(s) of AtYSL1 and AtYSL3 in the allocation of metals into various organs of Arabidopsis. AtYSL1 and AtYSL3 are localized to the plasma membrane, and each is capable of suppressing the growth defect of yeast lacking normal Fe uptake, indicating that the most likely biochemical

function for these proteins is in uptake of Fe(II)-NA complexes. We have used inflorescence grafting to determine the relative roles of AtYSL1 and AtYSL3 in leaves and inflorescences during seed development. These proteins are found to have dual roles: activity in the leaves is required for normal inflorescence development, while activity in the inflorescences themselves is required for proper loading of metals into the seeds. We have further examined the effect of overexpressing *AtYSL3*, which resulted in a small increase in Cu in shoots, and have demonstrated that the AtYSL1 protein, when expressed from the *AtYSL3* promoter, can only partially rescue the phenotypes of the *ysl1ysl3* double mutant, indicating that these proteins have distinct biochemical activities. A third *AtYSL* from the same subgroup of the *YSL* family, *AtYSL2*, also only partially complements the phenotypes of *ysl1ysl3* double mutants, suggesting that although these three YSL transporters are closely related, they have distinct activities in planta.

RESULTS

Suppression of Fe Growth Defects in Yeast Using *AtYSL1* and *AtYSL3*

An unusual phenomenon was observed while cloning *AtYSL3* cDNA for use in yeast functional complementation tests. We made at least seven independent attempts to clone *AtYSL3* cDNA, both by screening cDNA libraries and by reverse transcription (RT)-PCR. Clones were obtained in each attempt, but each time the cDNAs encoded only partial (in the case of clones derived from cDNA libraries; one attempt) or mutated versions of the cDNA (in the case of clones derived from RT-PCR; six independent attempts). Mutations were either induced through apparent polymerase errors during PCR that caused frame shifts (two independent cloning attempts) or by cloning of cDNA with one or two retained introns (four independent cloning attempts). These products are present in very low levels in our RT-PCRs; the vast majority of RT-PCR products are the correct size, and direct sequencing of PCR products confirms the presence of a large excess of fully spliced, expected cDNA product. We conclude that even low levels of expression of *AtYSL3* in *Escherichia coli* are causing lethality; thus, the only clones we obtained in *E. coli* were ones that do not encode AtYSL3 protein. We have made use of strains of *E. coli* that maintain plasmids at very low copy number (Copycutter, Epicenter), hoping that this would help to keep expression low and allow growth. However, this approach, too, was unsuccessful: only incorrectly sized clones with restriction patterns indicative of retained introns were obtained, and these were not further characterized by sequencing. Instead, we used direct cloning of *AtYSL3* in yeast through homologous recombination (Oldenburg et al., 1997), followed by sequencing to confirm that correctly spliced and nonmutated clones were obtained. This strategy completely circumvents the need for successful propagation of the *AtYSL3* cDNA in *E. coli*. The sequence of the cDNA clone we obtained in yeast has one change relative to the canonical At3g53550 sequence, a substitution replacing a positively charged Lys with another positively charged amino acid, Arg, in a weakly conserved region of the protein (Supplemental Fig. S1). Cloning of YSL1 cDNA was described previously (Waters et al., 2006).

We tested whether AtYSL1 and AtYSL3 are capable of transporting Fe-NA and Fe-PS complexes using a yeast phenotypic suppression (functional complementation) assay (Fig. 1). At least three independent replicates were used to confirm each assay. In this assay, *ferrous transport3/ferrous transport4* (*fet3fet4*) yeast were transformed with the *YSL*-expressing plasmids and

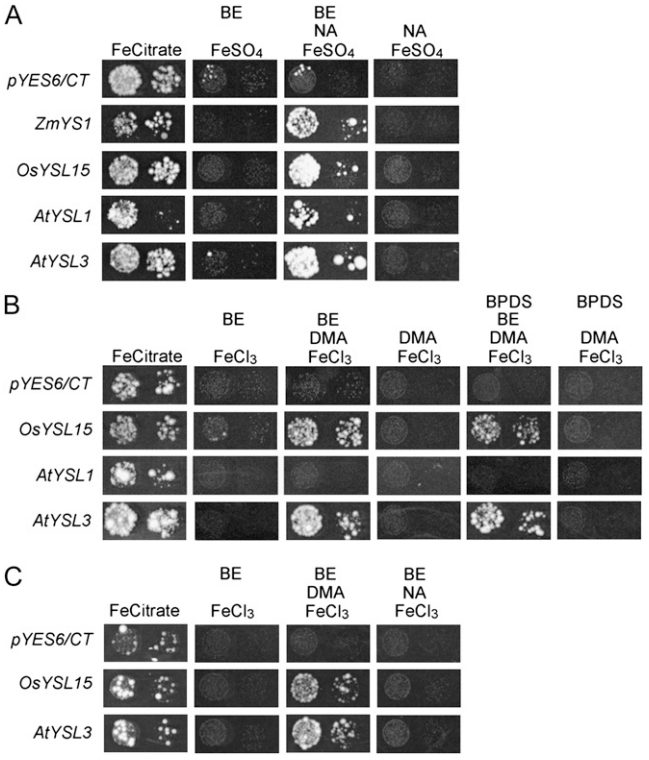

Figure 1. Functional complementation of *fet3fet4* yeast. DEY1453-derived yeast strains transformed with *pGEV-TRP* and constructs containing *AtYSL1*, *AtYSL3*, *OsYSL15*, or *ZmYS1* cDNA, or the empty *pYES6/CT* vector, were grown on synthetic defined medium containing variable conditions for Fe [Fe(II) or Fe(III)], chelator (DMA or NA), and β-estradiol (BE). Pairs of spots correspond to 10-fold and 100-fold dilutions of the original cultures. A, Results using Fe(II) and NA. Each plate contained the constituents indicated at the following concentrations: 50 μM Fe citrate, 3 μM Fe(II)SO_4, 8 μM NA, 10 nM BE. B, Results using Fe(III) and PS. Each plate contained the constituents indicated at the following concentrations: 50 μM Fe citrate, 10 μM Fe(III)Cl_3, 10 μM DMA, 40 nM β-estradiol. In addition, the Fe(II) chelator BPDS was added to some plates, as indicated. C, Results using Fe(III) and NA. Each plate contained the constituents indicated at the following concentrations: 50 μM Fe citrate, 10 μM Fe(III)Cl_3, 15 μM NA, 40 nM BE.

with the empty *pYES6/CT* vector, which serves as a negative control. Two positive controls, *ZmYS1* and/or *OsYSL15*, were also included. *OsYSL15* is the rice ortholog of *ZmYS1*, and like ZmYS1, OsYSL15 transports both Fe(II)-NA and Fe(III)-PS complexes (Inoue et al., 2009; Lee et al., 2009). To allow us to control the level of *YSL* expression in yeast, we made use of the β-estradiol-regulated expression system developed by Gao and Pinkham (2000). This system is used to achieve dose-dependent gene expression levels and further confers a tightly regulated off state, so that strains can be grown without expression of the target proteins (negative control). To demonstrate viability of the strains, all were grown under permissive conditions (50 μM Fe citrate; Fig. 1). When Fe(II) was provided in unchelated form (as 3 μM $FeSO_4$; Fig. 1A), both *AtYSL1* and *AtYSL3* failed to restore growth, but when NA was provided along with Fe(II) (3 μM $FeSO_4$ with 8 μM NA; Fig. 1A), suppression of the *fet3fet4* growth defect was observed for both strains. To demonstrate that growth is dependent on *YSL* expression, β-estradiol was withheld from the medium (Fig. 1A), and growth ceased. This result indicates that these genes encode transporters of Fe(II)-NA complexes.

To assay whether AtYSL1 and AtYSL3 transporters can use Fe(III)-PS as a substrate for transport, the strains were grown on 10 μM $FeCl_3$ and on 10 μM $FeCl_3$ plus 10 μM 2′-deoxymugineic acid (DMA; a PS; Fig. 1B), both in the presence of the inducer β-estradiol. Because Arabidopsis neither makes nor uses PS, neither *AtYSL* was expected to allow growth on Fe(III)-PS medium. Surprisingly, *AtYSL3* was able to complement growth in the presence of DMA but not on $FeCl_3$ alone, suggesting that this protein is able to transport Fe-PS complexes. As expected, *AtYSL1* failed to complement on medium containing Fe(III)-PS. To demonstrate that growth is dependent on *AtYSL3* expression, β-estradiol was withheld from the medium (Fig. 1B). Suppression of the *fet3fet4* growth defect on Fe(III)-PS still occurred when the strong Fe(II) chelator 4,7-biphenyl-1,10-phenanthroline-disulfonic acid (BPDS) was used to remove any residual Fe(II) from the Fe (III)-DMA medium (Fig. 1B), indicating that AtYSL3 transports Fe(III)-DMA. The ability of AtYSL3 to use Fe(III)-PS as a substrate could indicate that this transporter's in vivo substrate is Fe(III)-NA. To test this, we grew strains on medium that contained 10 μM $FeCl_3$ plus 15 μM NA (Fig. 1C), both in the presence of the inducer β-estradiol. Neither *AtYSL1* (data not shown) nor *AtYSL3* allowed growth on medium containing Fe (III)Cl_3 and NA.

Localization of Fe in *ysl1ysl3* Double Mutant Seeds

We have previously shown that the seeds produced by *ysl1ysl3* double mutants are low in Fe, Zn, and Cu (Waters et al., 2006). We used synchrotron x-ray fluorescence microtomography to visualize metals directly in seeds. In Arabidopsis seeds, Fe is most strongly localized to the provascular strands of the hypocotyl, radicle, and cotyledons (Kim et al., 2006). In seeds of *ysl1* and *ysl3* single mutants, localization of Fe (Fig. 2, B and C) is similar to that in the wild type. The amount of Fe in *ysl1* mutant seeds appears to be somewhat lower than in the wild type, consistent with previous analysis (Le Jean et al., 2005). The *ysl1ysl3* double mutant seeds have much reduced Fe (Fig. 2D; note scale). Double mutant seeds are small and frequently deformed (Waters et al., 2006), and the deformation of the seed shown is apparent (Fig. 2D). However, the pattern of Fe localization to the provascular strands of the cotyledons and radicle is retained in the double mutant when viewed without scaling relative to the other samples to allow clear visualization of the low levels of Fe that are present in the embryo (Fig. 2E). Owing to the deformation of the seeds of the double mutant, only five of the six provascular strands of the cotyledons are visible (three at top right, two at bottom right; Fig. 2E), and the provascular strand of the radicle is also present. Notice that a low Fe signal is present around the entire embryo (Fig. 2, A–D), and this is similar in amount in all four samples. Thus, the loss of AtYSL1 and AtYSL3 activity has no impact on the localization of Fe within Arabidopsis seeds, although the amount of Fe is markedly reduced.

Elemental values obtained via inductively coupled plasma mass spectroscopy (ICP-MS) and synchrotron x-ray fluorescence differ considerably, and comparison is not technically accurate. Volume-averaged methods average the values over the entire volume of the seed, and each value is the average of thousands of seeds. Spatially resolved metal analysis via a microprobe collects the abundance of one 10-μm-thick section of one seed, and depending on the heterogeneity of the element (which for Fe is high), the values differ widely. The localization of manganese (Mn), Cu, and Zn (Supplemental Fig. S2) in *ysl1* and *ysl3* single mutants, as well as in *ysl1ysl3* double mutants, was similar to that in the wild type, again indicating that deficiency for AtYSL1 or AtYSL3 does not disrupt the localization of these metals within the seeds, even though the levels of these metals are altered in the double mutants.

Localization of AtYSL1 and AtYSL3 Proteins in Planta

Both AtYSL1 and AtYSL3 are predicted to be plasma membrane proteins, and their activity in yeast (Fig. 1) is consistent with this localization, since yeast growth should rely on Fe transport across the plasma membrane. To determine the localization of AtYSL1 and AtYSL3 more conclusively, we made fusions of each gene to GFP. For *AtYSL1*, we placed a *AtYSL1* cDNA clone under the control of the *35S* promoter and fused GFP at the C terminus of the protein (*35S-YSL1-GFP*). This construct was introduced into onion (*Allium cepa*) skin cells using microprojectile bombardment (Fig. 3, A–C). The pattern of fluorescence observed for the *AtYSL1-GFP* fusion protein is consistent with localization to the plasma membrane: the signal is at the periphery of the cell and does not deviate around the

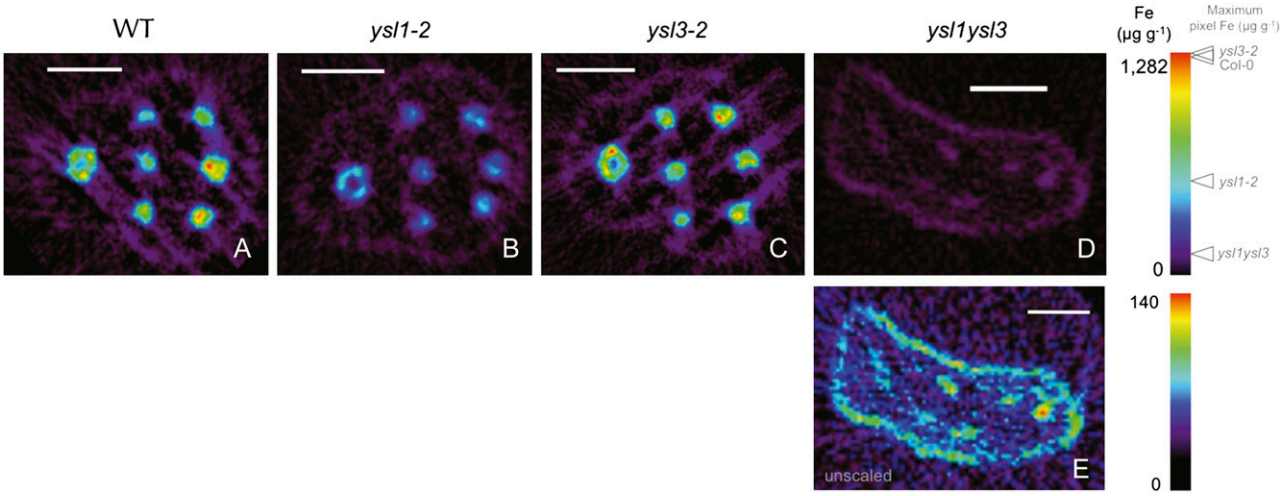

Figure 2. Synchrotron x-ray fluorescence computed microtomography showing the distribution and abundance (in μg g^{-1}) of Fe. Tomograms (virtual cross-sections) were collected via synchrotron x-ray fluorescence computed microtomography from intact, dry Arabidopsis seeds. In each panel, the embryonic radicle is at the left and the cotyledons are at the right. A single provascular strand is visible in the radicle, and three provascular strands are visible in each cotyledon. A, Wild-type (WT) Col-0. Bar = 100 μm. B, *ysl1-2* mutant. Bar = 100 μm. C, *ysl3-1* mutant. Bar = 100 μm. D, *ysl1ysl3* double mutant. Bar = 100 μm. E, *ysl1ysl3* double mutant shown without scaling relative to the other specimens. Bar = 100 μm.

nucleus (Fig. 1). As a positive control for cytosolic localization, we bombarded with a construct containing soluble GFP under the control of a *35S* promoter (*35S-smGFP*; Fig. 3, D–F). Fluorescence was observed in the cytosol and nucleus, as expected. For AtYSL3 localization, the whole gene, including its native promoter, was fused to GFP, again at the C terminus (*YSL3-GFP*). As a control for tonoplast localization, a construct containing the gene for the tonoplast-localized protein TIP1 was also examined. Arabidopsis plants were stably transformed with these constructs, and the fluorescence patterns were observed in roots of the transformed plants. The signal from YSL3-GFP is again located at the periphery of the cells and does not deviate around nuclei (Fig. 3, G–I). By contrast, the TIP1 signal deviated around nuclei as expected for a tonoplast protein (Fig. 3, J–L, arrows). For AtYSL3, green fluorescence was strongest in elongated cells within the vasculature of both leaves (data not shown) and roots (Fig. 3, G–I), apparently xylem parenchyma. Strikingly, fluorescence for AtYSL3 was only rarely observed at the apical or basal end of cells but was instead found almost exclusively on the lateral plasma membranes. This pattern is very similar to that of AtYSL2 (DiDonato et al., 2004) and suggests similar functions for these two closely related proteins. This pattern is consistent with a role for these proteins in the lateral movement of metals within veins.

Grafting of *ysl1ysl3* Inflorescences

As noted above, reproduction of *ysl1ysl3* double mutants is impaired (Waters et al., 2006). Pollen function is severely reduced, and seed development is incomplete in most cases. In addition, seeds produced by *ysl1ysl3* double mutant plants contained reduced levels of Zn and Cu, the same metals that failed to be mobilized out of the leaves. The double mutant seeds also contained reduced levels of Fe. We hypothesized that the reduced levels of metals in the seeds produced by *ysl1ysl3* double mutants result from decreased metal translocation into reproductive structures from senescing leaves (Waters et al., 2006). To investigate further, we grafted young (approximately 3–7 cm) primary inflorescence stems of *ysl1ysl3* double mutant plants onto wild-type plants and then allowed flowering and seed set to proceed. If the metal levels of the seeds are dependent on the function of AtYSL1 and AtYSL3 in the vegetative parts of the plant, grafting should rescue the reproductive phenotypes of the double mutant. As a control, we also made self-grafts of wild-type plants. We attempted to perform self-grafts of the *ysl1ysl3* double mutants, as well as grafts of wild-type inflorescences onto *ysl1ysl3* rosettes, but were not able to obtain viable grafts in spite of repeated attempts. Therefore, we present comparative data obtained from ungrafted double mutant plants. Visual inspection of the grafted *ysl1ysl3* flowers indicated that anther stunting was alleviated and pollen was released from anthers of the grafted flowers. The measures of seed set (a quantitative proxy for pollen function, since nonfunctional pollen results in failure of seed set; Fig. 4A) and seed weight (Fig. 4B) indicate that AtYSL1 and AtYSL3 function is required in leaves for normal pollen and seed development. Both seed set and seed weight from the grafted plants were significantly higher than from ungrafted double mutant plants and were furthermore not significantly different

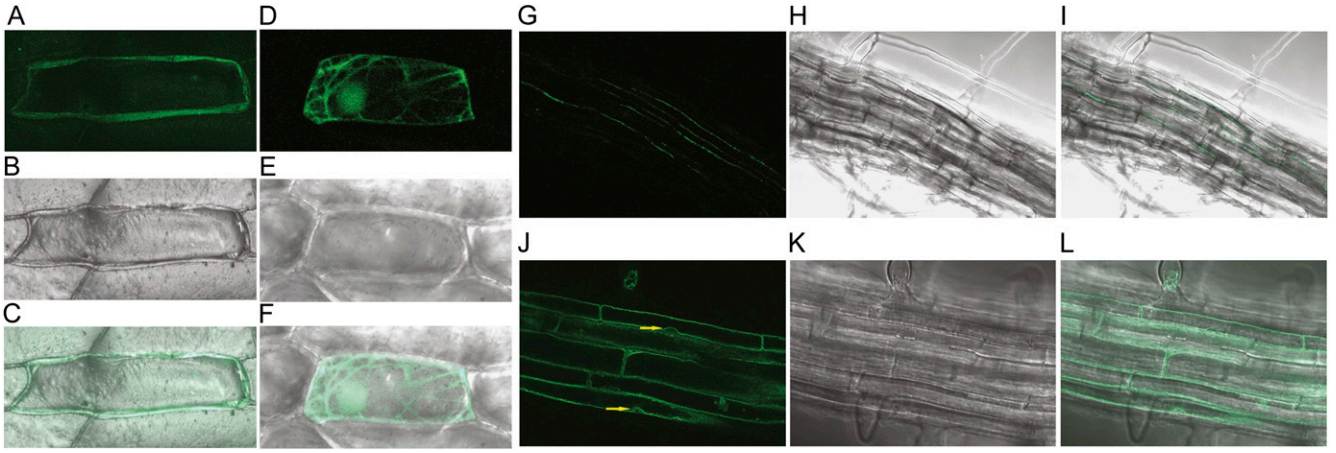

Figure 3. Localization of AtYSL1 and AtYSL3 using GFP. A to F, Localization in onion epidermal cells using microprojectile bombardment. G to L, Localization in stably transformed Arabidopsis. Fifteen optical sections were fused to produce each micrograph. A, Fluorescence image of an onion cell bombarded with the *35S-YSL1-GFP* construct. B, Differential interference contrast (DIC) image of the onion cell shown in A. C, Overlay of images shown in A and B. D, Fluorescence image of an onion cell bombarded with the *35S-smGFP* construct. E, DIC image of the onion cell shown in D. F, Overlay of images shown in D and E. G, Fluorescence image of the root of a plant stably transformed with the *YSL3-GFP* construct. H, DIC image of the root shown in G. I, Overlay of images shown in G and H. J, Fluorescence image of the root of a plant stably transformed with the *35S-TIP* construct. Arrows indicate positions where the fluorescence signal deviates around nuclei. K, DIC image of the root shown in J. L, Overlay of images shown in J and K.

from wild-type self-grafts (by Student's *t* test). These results indicate that AtYSL1 and AtYSL3 functions are required in the rosettes (stems/leaves/roots) to accomplish normal pollen and seed development.

We also tested whether the *ysl1ysl3* seeds produced by grafted inflorescences would germinate normally. Seeds from ungrafted double mutant plants show severe germination defects on soil (Waters et al., 2006; Fig. 4C), with only 31% of seeds germinating. By contrast, germination of seeds produced from grafted inflorescences (89%) was not significantly different from seeds of wild-type self-grafts (91%).

We measured the metal content of the seeds produced by ungrafted wild-type plants, wild-type self-grafts, *ysl1ysl3* grafts to wild-type plants, and ungrafted *ysl1ysl3* plants. By contrast to the rescue of pollen function, seed development, and germination caused by grafting, the contents of Fe, Zn, and Cu in the seeds from grafted plants remained low (Fig. 5). For each of these metals, there was a trend toward the normal metal level in the *ysl1ysl3* seeds that developed from the grafted inflorescences. However, the metal levels of the seeds produced from grafted *ysl1ysl3* stems were not significantly different (by Student's *t* test) from the metal levels in seeds of the ungrafted double mutant plants. Seeds from both grafted and ungrafted *ysl1ysl3* inflorescences were significantly lower than ungrafted wild-type plants and wild-type self-grafts with respect to Cu and Zn. The Fe levels of seeds produced by ungrafted *ysl1ysl3* plants were not significantly lower than wild-type levels, but the Fe levels of seeds from the grafted *ysl1ysl3* inflorescences were significantly lower than those of wild-type plants or wild-type self-grafts. These results indicate that AtYSL1 and AtYSL3 functions are required in the grafted portion of the plants (i.e. in the inflorescence stems or cauline leaves, the flowers themselves, or the developing fruits and seeds) in order for the seeds to contain normal metal levels at maturity. By comparing ungrafted wild-type plants with wild-type self-grafts, we were able to observe that grafting caused a large decrease the Mn content of the seeds produced by grafted branches, but the other metals measured in this study were not affected by grafting per se.

Phloem Suc Concentrations in *ysl1ysl3* Double Mutants

The normal development of pollen and seeds in *ysl1ysl3* grafts caused us to question whether the recovery of pollen and seed development is caused by YSL-mediated movement of metals or by an indirect effect on bulk flow in phloem. Since *ysl1ysl3* double mutants are chlorotic, they presumably have lower than normal rates of photosynthesis and thus may export less sugar via phloem. Lower sugar transport could have two distinct effects. One is that, to drive phloem transport of Fe to the seeds, adequate Suc in the phloem is required. In this model, pollen and seed defects could be the result of reduced metal translocation that is a secondary effect from generally defective phloem transport. Alternatively, sugar itself must be needed for pollen and seed development; thus, the simple lack of carbohydrate experienced by the chlorotic *ysl1ysl3* plants could be the cause of the pollen and seed defects.

Previously published experiments in which *ysl1ysl3* double mutants were treated with ferric ammonium

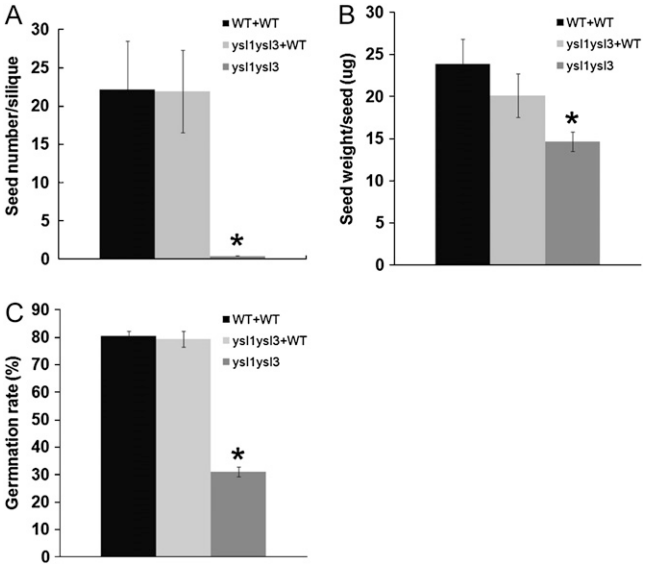

Figure 4. Inflorescence grafting experiment. *ysl1ysl3* double mutant scions (inflorescences) grafted onto wild-type stocks are labeled as *ysl1ysl3*+WT. WT+WT indicates wild-type plants that were self-grafted as positive controls. *ysl1ysl3* double mutant was used as a negative control, since it was not possible to generate self-grafted *ysl1ysl3* plants. Error bars represent SD. Asterisks indicate $P < 0.05$ by *t* test. A, Average seed number per silique. Each silique on the grafted inflorescences was opened, and the seed number was counted. WT+WT and *ysl1ysl3* samples contain four replicates, and *ysl1ysl3*+WT sample contains six replicates. B, Average weight of an individual seed produced by the grafted inflorescences. WT+WT and *ysl1ysl3* samples contain four replicates, and *ysl1ysl3*+WT sample contains six replicates. C, The percentage of seeds germinating on soil was determined. Four replicate batches of 100 of each seed type were used in the analysis. Germination was defined as emergence of the radicle and was scored every 24 h after plating.

citrate (Waters et al., 2006) can be used to address the concern that pollen and seed failure result from a lack of carbohydrate. Ferric ammonium citrate treatment corrected the chlorosis of *ysl1ysl3* double mutants, suggesting restored photosynthesis in treated double mutant leaves. However, ferric ammonium citrate treatment only weakly affected plant fertility. In this experiment, normal photosynthesis in leaves but loss of function of *AtYSL1* and *AtYSL3* results in poor recovery of pollen and seed development, strongly suggesting that it is metal transport, not sugar production, that causes the pollen and seed weight defects of the double mutant. To support this idea, we measured the level of Suc in the phloem of wild-type and *ysl1ysl3* plants (Fig. 6). The Glc content in the phloem exudates was below the detection limit (50 nmol g^{-1} fresh weight; data not shown), suggesting that the contamination caused by cell damage in the exudates is low. The amount of Suc in the phloem of the double mutants did not differ from that in wild-type plants, suggesting that Suc translocation and bulk flow in the phloem of the double mutants is normal.

Overexpression of *AtYSL3* in Planta

Overexpression is an important tool that can be used to determine the function of a gene. To accomplish overexpression, the gene is typically placed under the control of a strong constitutive promoter to cause high expression levels in most or all cells. This approach did not work well for *AtYSL* genes, as this type of overexpression gave rise to seedlings that did not thrive and did not produce consistent phenotypes (data not shown). As an alternative, we added multiple copies of the *35S* enhancer to the native *AtYSL3* promoter, which then drives expression of the downstream gene. This arrangement is expected to lead to an enhancement of expression but in the normal location(s), without causing ectopic expression (Weigel et al., 2000; Mora-Garcia et al., 2004; Tian et al., 2004). Quantitative RT-PCR experiments demonstrated that only one of three overexpression lines tested had increased mRNA levels in leaves (Fig. 7A). Expression in cauline leaves and in the flowers and flower buds was close to normal (Fig. 7, B–D). To determine whether overexpression of *AtYSL3* in vegetative tissues caused changes in metal accumulation, we examined the levels of metals in vegetative leaves (Fig. 7E) and in seeds (Fig. 7F). In all three lines, the Cu levels of the leaves were significantly higher than normal. Fe and Zn levels were not affected in the overexpression lines. In addition, the leaf Mn level of only a single line (7.1) was affected. In the seeds, no significant changes in the level of any metal were observed, with one exception: one line produced seeds with a small but significant decrease in Zn. However, since the Mn and Zn changes were only associated with a single line, and moreover did not correlate with expression levels, their importance is not clear. The lack of clear changes in metal content in seeds may reflect the weak or nonexistent

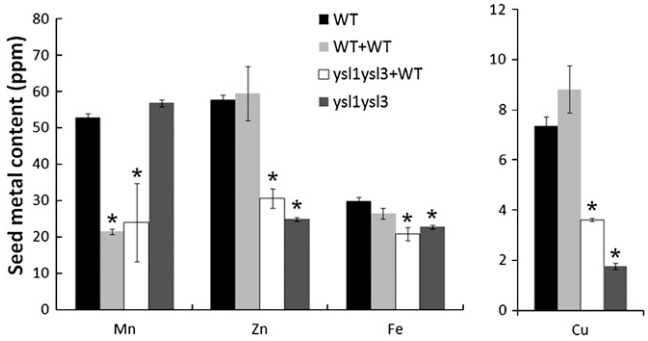

Figure 5. Metal concentration of seeds of grafted plants. Metal content of the seeds produced by ungrafted wild-type plants (WT), by wild-type self-grafted plants (WT+WT), by *ysl1ysl3* inflorescences grafted to wild-type rosettes (*ysl1ysl3*+WT), and by *ysl1ysl3* ungrafted plants was determined using ICP-MS. As a control for the effect of inflorescence grafting on seed metal concentration, seeds from ungrafted wild-type plants were also measured. WT+WT and *ysl1ysl3* samples contain four replicates, *ysl1ysl3*+WT sample contains six replicates, and ungrafted wild-type sample contains 10 replicates. Asterisks indicate $P < 0.05$ by *t* test.

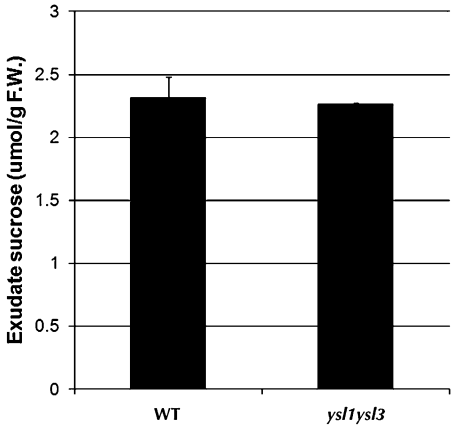

Figure 6. Suc levels in the phloem of wild-type (WT) and *ysl1ysl3* double mutant plants. F.W., Fresh weight.

overexpression indicated by RT-PCR results from flowers, buds, and especially cauline leaves.

In an effort to uncover subtle phenotypes associated with overexpression of *AtYSL3*, and because overexpression of *AtYSL3* was strongest in vegetative tissues, we examined whether the lines were resistant or sensitive to Fe deficiency stress. In this experiment, seeds were germinated on Murashige and Skoog (MS) medium that lacked Fe, and the total chlorophyll level of the seedlings, which reflects the level of Fe deficiency chlorosis, was measured at various time points. Line 5.8, which had the highest expression level for *AtYSL3* mRNA (Fig. 7A), was mildly resistant to prolonged Fe deficiency, with significantly higher chlorophyll levels at later time points (i.e. 18–24 d of Fe starvation; Fig. 7G). The two lines with weaker expression showed no significant differences from wild-type Columbia-0 (Col-0) plants.

Complementation of *ysl1ysl3* Double Mutants by Other *YSL* Genes

The YSL family contains three well-conserved clades that are present in all plants (Curie et al., 2009). A key question concerning the YSL family is whether each member has a distinct biochemical function or instead whether closely related members of the family share overlapping biochemical functions and differ only in their expression patterns. AtYSL1 and AtYSL3 both belong to the same clade and so might have similar or identical biochemical functions. This model explains the mild phenotype of the single *ysl1* mutant (Le Jean et al., 2005) compared with the severe phenotype of *ysl1ysl3*: the two genes could have overlapping expression patterns but encode functionally equivalent proteins. This does not completely explain the *ysl1ysl3* phenotype, however, because in flowers, fruits, and seeds there is little or no overlapping expression between *AtYSL1* and *ATYSL3*; thus, straightforward functional redundancy may not explain these attributes of the double mutants.

To test this, we used a complementation approach in which a cDNA encoding *AtYSL1* was placed under the control of the *AtYSL3* promoter, and the resulting construct was used to transform *ysl1ysl3* double mutant plants. If AtYSL1 and AtYSL3 have highly similar (or identical) biochemical functions, then the phenotypes associated with the double mutant (chlorosis, infertility, poor seed viability) should be alleviated or reversed. Complementation using *YSL3p*:*YSL1* provided only partial rescue of the phenotypes associated with the *ysl1ysl3* mutant. Chlorophyll levels in four independent lines were intermediate between those of the wild type and the uncomplemented double mutant (Fig. 8, A and B) and were significantly (by Student's *t* test) different from both. Thus, *AtYSL1* can only partially complement *AtYSL3* transport function in planta. The reciprocal experiment (*AtYSL1* promoter driving *AtYSL3* expression) was not performed, because *AtYSL3* cDNA cannot be maintained in *E. coli* and thus cannot be readily manipulated to generate the appropriate construct. However, a positive control, a *AtYSL3* genomic clone that was fused to GFP for localization studies and that contains the same promoter as used in this experiment, has been used to transform the double mutant, and it complements the chlorotic double mutant phenotype completely (Fig. 8C).

Complementation of reproductive phenotypes using *YSL3p*:*YSL1* was even less successful (Fig. 8, D and E). The construct used was not able to correct seed development (seed weight; Fig. 8D), since the seeds produced by plants containing *YSL3p*:*YSL1* were the same weight as double mutant seeds. In addition, the fertility defect of the plants was not corrected by the *YSL3p*:*YSL1* transgene; plants carrying the construct produced a similar number of seeds as the double mutant plants. Both seed amount and seed weight were normal in *ysl1ysl3* plants complemented with *YSL3*::*GFP* (data not shown). Thus, *AtYSL1* and *AtYSL3* appear to have related but distinct functions in planta.

A third Arabidopsis *YSL* family member, *AtYSL2*, is present in the clade that contains *AtYSL1* and *AtYSL3*. The pattern of expression of *AtYSL2* is similar to that of *AtYSL1* and *AtYSL3* in that expression is strongest in leaf veins and is negatively regulated by Fe deficiency. Also like AtYSL1 and AtYSL3, AtYSL2 is a plasma membrane protein and is capable of transporting Fe(II)-NA (DiDonato et al., 2004). Thus, we tested whether *AtYSL2* could substitute for *AtYSL3* in the double mutant by constructing a *YSL3p*:*YSL2* gene in which *AtYSL2* cDNA is driven by the *AtYSL3* promoter. In three independent lines carrying this construct (in a *ysl1ysl3* double mutant background), chlorophyll levels were intermediate between wild-type Col-0 and *ysl1ysl3* mutants, indicating that *AtYSL2* only partially complements *AtYSL3* function (Fig. 8, A and B). Both seed weight and seed production were unimproved in *ysl1ysl3* plants carrying the *YSL3p*:*YSL2* construct (Fig. 8, D and E). Thus, *AtYSL2*

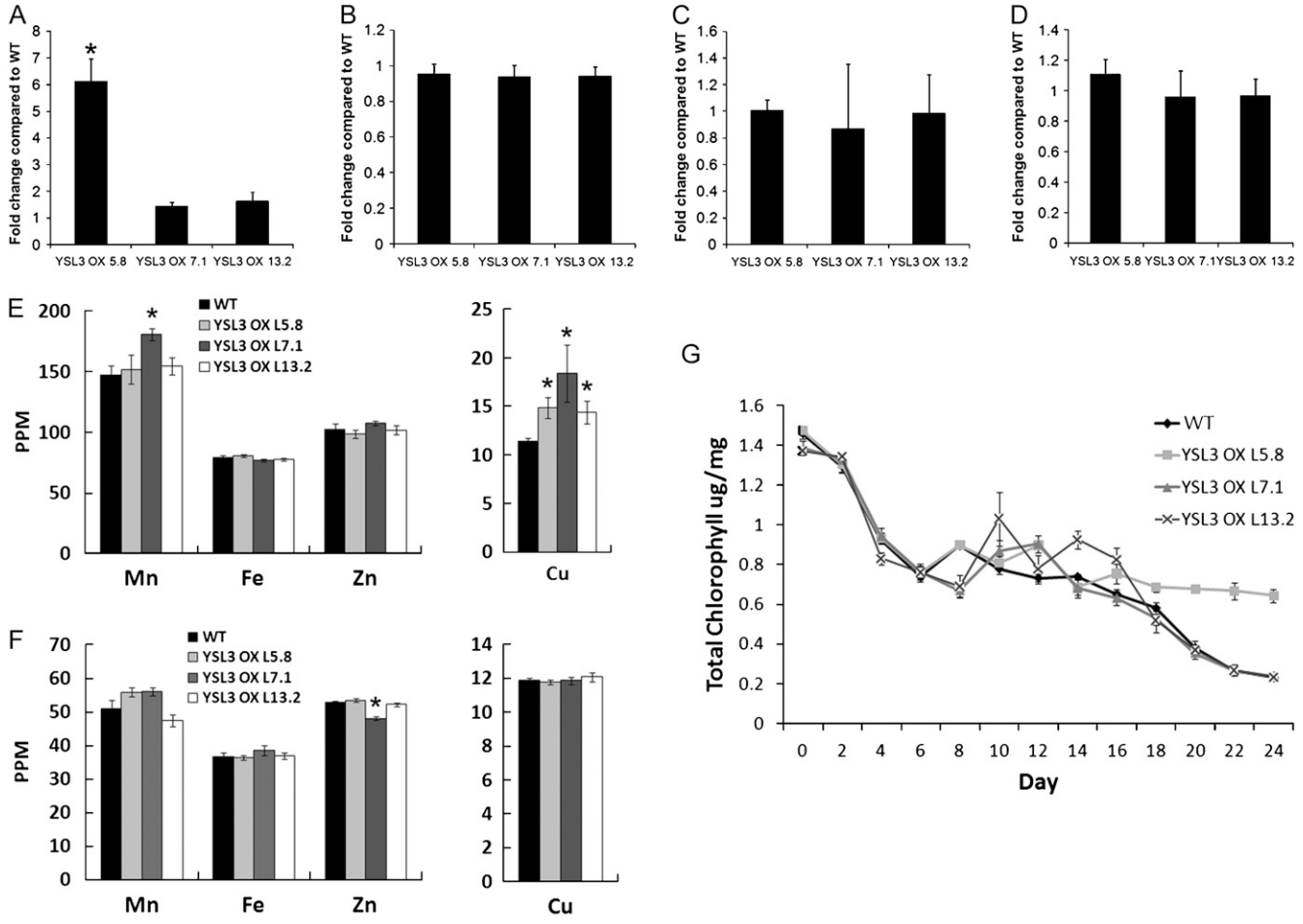

Figure 7. *AtYSL3* enhanced expression lines YSL3 OX L5.8, YSL3 OX L7.1, and YSL3 OX L13.2. Each line contains a *4X35S* enhancer sequence upstream of a *AtYSL3* genomic clone containing 1,487 bp of native *AtYSL3* sequence upstream of the initiating ATG. A to D, Expression of *AtYSL3* by quantitative RT-PCR. Values were normalized to corresponding *Actin2* values and expressed as fold induction relative to wild-type (WT) plants. A, Leaves. B, Flowers. C, Flower buds. D, Cauline leaves. E, ICP-MS determination of Mn, Fe, Cu, and Zn concentrations of leaves from 20-d-old soil-grown plants. Results are given as ppm (μL L^{-1}). Error bars represent SE. Each sample contains 10 replicates. Asterisks indicate $P < 0.05$ by *t* test. F, ICP-MS determination of Mn, Fe, Cu, and Zn concentrations of seeds. Results are given as ppm (μL L^{-1}). Error bars represent SE. Each sample contains 10 replicates. Asterisks indicate $P < 0.05$ by *t* test. G, Fe starvation response in wild-type and *AtYSL3* enhanced expression lines YSL3 OX L5.8, YSL3 OX L7.1, and YSL3 OX L13.2. Plants were grown on MS plates for 10 d and then transferred to MS medium without Fe for a period of 0 to 24 d. The total chlorophyll content of the shoot system was measured every 2 d.

and *AtYSL3* also appear to have related but distinct functions in planta.

DISCUSSION

Reproduction Requires YSL1 and YSL3 in Distinct Locations

An accepted model for nutrient loading into seeds (Hocking and Pate, 1977, 1978) suggests that metals mobilized from vegetative structures account for 20% to 30% of the metal content of seeds. Thus, starting from the simple hypothesis that YSL1 and YSL3 activity in leaves allows metal movement from senescing leaves into seeds, we performed grafting experiments that separated gene expression in the reproductive structures (inflorescence stems containing cauline leaves, flowers, fruits, and seeds) from gene expression in the vegetative structures (rosettes and roots). By doing this, we uncovered a more complex pattern than was initially anticipated. Expression of YSL1 and YSL3 in the rosettes and roots is necessary for successful formation of pollen and for completion of seed development (Fig. 4), suggesting that metals that are translocated from senescing leaves are used for the manufacture of reproductive structures. However, YSL1 and YSL3 are also required more locally (within the inflorescences) in order for loading of metals into the seeds to proceed normally (Fig. 5). These data indicate that short-range translocation within the inflorescence itself is more important than long-range translocation from shoot or root to inflorescence for

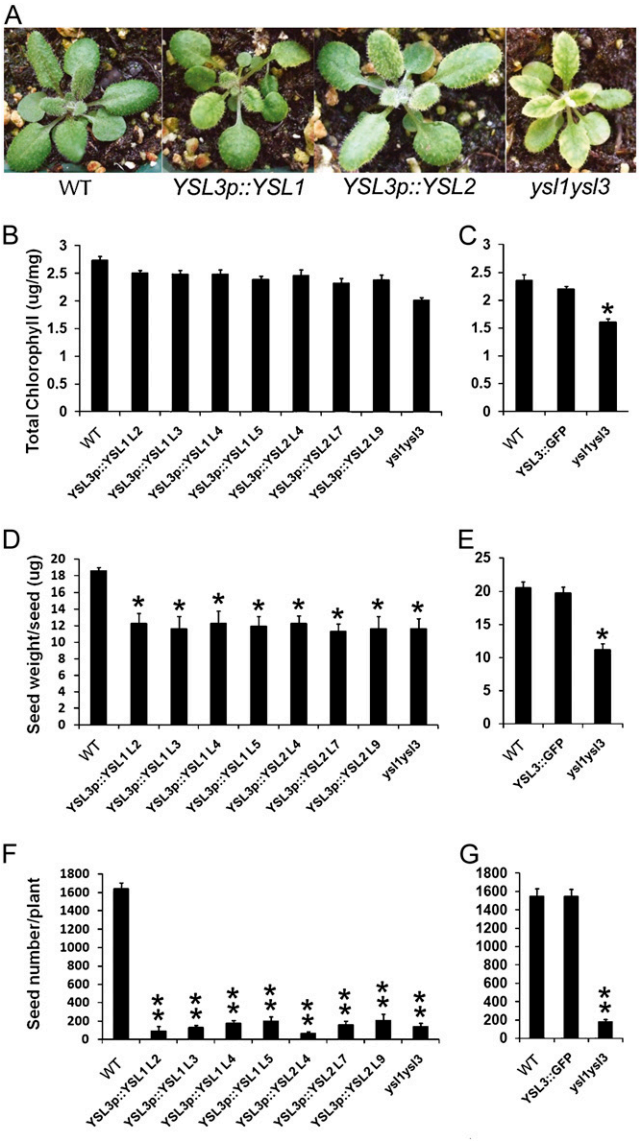

Figure 8. Complementation of *ysl1ysl3* double mutants with *AtYSL1* and *AtYSL2*. *ysl1ysl3* double mutant plants were transformed with *AtYSL1* and *AtYSL2* cDNA driven by the *AtYSL3* promoter (*YSL3p*::*YSL1* and *YSL3p*::*YSL2*) or with a *YSL3* genomic clone fused to GFP (*YSL3-GFP*). Four lines of *YSL3p*::*YSL1* (L2, L3, L4, and L5) and three lines of *YSL3*::*YSL2* (L4, L7, and L9) were included. Single asterisks indicate $P < 0.05$ by *t* test, and double asterisks indicate $P < 0.01$ by *t* test. A, Twenty-day-old soil-grown Col-0 wild-type (WT), *YSL3p*::*YSL1*, *YSL3p*::*YSL2*, and *ysl1ysl3* plants. B, Total chlorophyll concentration of leaves of Col-0 wild-type, *YSL3p*::*YSL1*, *YSL3p*::*YSL2*, and *ysl1ysl3* plants grown on soil for 20 d. Each sample represents 10 replicates. C, Total chlorophyll concentration of leaves of Col-0 wild-type, *YSL3*::*GFP*, and *ysl1ysl3* plants grown on soil for 20 d. D, Average weight of individual seeds of Col-0 wild-type, *YSL3p*::*YSL1*, *YSL3p*::*YSL2*, and *ysl1ysl3* plants. E, Average weight of individual seeds of Col-0 wild-type, *YSL3*::*GFP*, and *ysl1ysl3* plants. F, Average seed number per plant for Col-0 wild-type, *YSL3p*::*YSL1*, *YSL3p*::*YSL2*, and *ysl1ysl3* plants. G, Average seed number per plant for Col-0 wild-type, *YSL3*::*GFP*, and *ysl1ysl3* plants.

metal deposition into seeds. In previous work (Waters et al., 2006), we showed that *YSL1* and *YSL3* are poorly expressed in flowers, fruits, and seeds, and moreover that their expression does not overlap in these structures, suggesting that YSL1 and YSL3 activity within these structures is unlikely to be responsible for loading of metals to seeds. Instead, we propose that it is activity in the cauline leaves or the inflorescence stems that is required for the short-distance translocation of metals into the seeds themselves. According to publicly available microarray data and our own unpublished results, both YSL1 and YSL3 are strongly expressed in cauline leaves and moderately expressed in inflorescence stems, making these structures excellent candidates for key sites of metal export for retranslocation into developing seeds in Arabidopsis.

This model is consistent with the results of classic experiments performed by Grusak (1994), who demonstrated that Fe applied to the pod wall of pea (*Pisum sativum*) was rapidly retranslocated into developing seeds, and with more recent experiments examining whole-plant dynamics of mineral flow (Waters and Grusak, 2008). In addition, our finding that the seeds of the grafted plants have normal germination in spite of their lower Fe, Zn, and Cu levels indicates that the germination defects of the double mutant are likely due to seed developmental arrest, not to metal content per se.

Formally, failure of pollen and seed development in the double mutant could result from aberrant metal homeostasis or, alternatively, could arise from diminished sugar translocation resulting from reduced photosynthetic capacity of the chlorotic double mutants. Lower sugar transport could have two distinct effects. One is that, to drive phloem transport of Fe to the seeds, adequate Suc in the phloem is required. In this model, pollen and seed defects could be the result of reduced metal translocation that is a secondary effect from generally defective phloem transport. Alternatively, sugar itself must be needed for pollen and seed development; thus, a simple lack of carbohydrate in chlorotic *ysl1ysl3* plants could be the cause of the pollen and seed defects. We found that the level of Suc in the phloem of the double mutant plants was similar to the wild-type level, suggesting that low carbohydrate is not causing reproductive phenotypes. Moreover, ferric ammonium citrate treatment corrected the chlorosis of *ysl1ysl3* double mutants, suggesting restored photosynthesis but only weakly affected plant fertility, again suggesting that it is metal transport, not sugar production, that causes the pollen and seed weight defects of the double mutant (Waters et al., 2006). We conclude that pollen and seed development in the double mutant fails because metal transport from senescing leaves is defective.

The Transporter Activity of AtYSL1 and AtYSL3 in Yeast

Here, we have shown that *AtYSL1* and *AtYSL3* suppress the Fe-specific growth defect of the yeast *fet3fet4* mutant, indicating that these YSLs are Fe

transporters. In previous work, we used a noninducible expression system for functional testing of YSL proteins using yeast growth complementation (DiDonato et al., 2004). However, the vector used, *pFL61*, caused unanticipated growth changes in the alternative yeast strain (*ftr1*) used in similar experiments conducted by other groups (Schaaf et al., 2005). In this work, by carefully controlling *YSL* expression from a β-estradiol-inducible promoter, we have demonstrated that growth is dependent on both expression of each *YSL* gene and the presence of the appropriate chelator (NA or PS). In medium with an equal amount of Fe but no chelator, growth limitation occurs. In medium with an equal amount of chelator and Fe, but without β-estradiol, growth limitation occurs. This strongly implies that Fe-NA or Fe-PS complexes are required by these YSLs as substrates for transport. Although Fe(II)-NA transporter activity was expected for AtYSL1 and AtYSL3, it was surprising to find that Fe(III)-PS is apparently a usable substrate for transport by AtYSL3, since PS, including DMA used in the assay, are not produced by Arabidopsis. Only grass species (e.g. rice, maize, wheat, etc.) produce PS, so only these species would be expected to have YSLs that transport PS. One explanation for this activity of AtYSL3 is that this protein might possess the ability to transport Fe (III) bound to NA. Fe(III)-NA complexes are expected to occur in all plants (von Wiren et al., 1999), including Arabidopsis, and DMA, being structurally very similar to NA, could be substituting for NA to form a transportable complex. When medium containing both Fe (III) and NA were used in the growth assay, no functional complementation was observed. This negative result leaves the question of Fe(III)-NA transport via AtYSL3 open, since the failure of complementation could reflect a true lack of this transport activity for AtYSL3 or could reflect a problem with the assay conditions [e.g. if Fe(III)-NA complexes do not form or are unstable under the conditions used in the complex medium needed for yeast growth]. Since AtYSL3 appears to possess a distinct biochemical function that cannot be completely replicated by AtYSL1 or AtYSL2 (see below), it is tempting to speculate that the latter explanation may be correct.

The *ysl1ysl3* double mutants exhibit marked alterations in Zn and Cu homeostasis, especially in the seeds but also in leaves during senescence (Waters et al., 2006). This could come about because of a direct effect in which AtYSL1 and AtYSL3 are transporters of these metals, or it could be an indirect effect in which altered Fe homeostasis causes secondary effects on the levels of other metals. We have also examined whether AtYSL1 and AtYSL3 are capable of transporting Zn-NA complexes and Cu-NA complexes using yeast functional complementation with strains defective in Cu or Zn uptake, but we have not observed any evidence of Cu or Zn uptake (data not shown), although the AtYSL2 protein does appear to transport Cu-NA in these assays (DiDonato et al., 2004). We are reluctant to ascribe any functional significance to these negative results. Additional assay systems must be developed before a conclusion can be reached regarding the capacity of these proteins to move substrates other than Fe(II).

Functional Equivalency of YSL Transporters in Planta

We have also examined the functional equivalency of the three proteins in the YSL1/YSL2/YSL3 clade of Arabidopsis and find that these proteins, in spite of their strong, full-length sequence similarity (AtYSL1 and AtYSL2 are 79% similar; AtYSL2 and AtYSL3 are 86% similar), do not completely functionally complement each other's activities in planta. Partial complementation of AtYSL3 activity was observed in vegetative structures, where expression of *AtYSL1* and *AtYSL2* from the *AtYSL3* promoter produced plants that were less chlorotic than the parent *ysl1ysl3* double mutant line. The partial complementation observed is consistent with the strong overlap in expression of AtYSL1 and AtYSL3 in leaves (Waters et al., 2006). By contrast, *AtYSL1* and *AtYSL2* were completely unable to substitute for *AtYSL3* with respect to reproductive function. This result implies that AtYSL3 has a distinct activity required for successful reproduction, which is not present in the closely related AtYSL1 and AtYSL2 proteins. It is tempting to speculate that this activity relates to AtYSL3's apparent ability to transport Fe(III) in addition to Fe(II), but one could also speculate that failure to complement is the result of other transport properties that have not yet been determined, for example, the ability to transport Fe-NA complexes both into and out of cells.

MATERIALS AND METHODS

Plant Growth Conditions

Arabidopsis (*Arabidopsis thaliana*) seeds were surface sterilized in 70% ethanol with 0.05% Triton X-100 and then imbibed in sterile distilled water at 4°C for 3 to 5 d. Plants were grown on sterile plates containing 1× MS medium. Plates were positioned vertically so that the roots grew along the surface rather than inside the agar, which allowed for easy transfer. Soil-grown plants were sown directly onto Metro-Mix (Sungro Horticulture) treated with Gnatrol (Valent Biosciences) to control fungus gnats. Growth chamber conditions for plates and soil-grown plants were 16 h of light and 8 h of dark at 22°C.

Cloning of *YSL3* cDNA

YSL3 cDNA was amplified by RT-PCR using Platinum Taq DNA Polymerase High Fidelity (Invitrogen) and the following primers: oAtYSL3-c.39..65y (5′-ATCCACTAGTAACGGCCGaaatgaggagtatgatgatggagagag-3′) and oAtYSL3.4203..4198y (5′-CCGCCACTGTGCTGGATAtctgtaactcgaatatttactcggcat-3′). Each primer contains an 18-nucleotide (lowercase) overlap with yeast expression vector pYES6/CT for in vivo homologous recombination. *YSL3* cDNA and linearized pYES6/CT were cotransformed into Fe-uptake-defective yeast strain DEY1453, and recombinant plasmids were selected using blasticidin resistance.

Yeast Functional Complementation

Saccharomyces cerevisiae strain DEY1453 (MATa/MATa ade2/ADE2 can1/can1 his3/his3 leu2/leu2 trp1/trp1 ura3/ura3 fet3-2::HIS3/fet3-2::HIS3 fet4-

1::LEU2/fet4-1::LEU2) was transformed with *pGEV-Trp* (Gao and Pinkham, 2000) together with pYES6/CT or pYES6/CT with AtYSL1 or AtYSL3 cDNA. For complementation assays, SD-Trp medium was made with Fe-free yeast nitrogen base buffered with 25 mM MES at pH 5.7 [for plates containing Fe(II)] or pH 6.0 [for plates containing Fe(III)]. To prepare assay plates containing Fe (II), the following were added, in order, to the center of an empty plate: 125 μL of 200 mM ascorbic acid, 7.5 μL of freshly prepared Fe(II)SO_4, and 20 μL of 10 mM NA. The solution was mixed briefly and incubated at room temperature for 10 min to allow complex formation. Following this, 25 mL of molten SD-Trp with 10 μg mL^{-1} blasticidin was added to the plates and was then allowed to solidify. On plates containing β-estradiol, the stock solution was added to the molten agarose just prior to preparation of the plates. To prepare assay plates containing Fe(III), 34 μL of 7.4 mM $FeCl_3$ and 25 μL of 10 mM DMA or 10 mM NA were placed at the center of an empty plate and incubated at room temperature for 10 min to allow complex formation. Following this, 25 mL of molten SD-Trp with 10 μg mL^{-1} blasticidin was added to the plates and was then allowed to solidify. When preparing plates with BPDS, 25 μL of 10 mM BPDS was added just prior to the addition of molten medium. NA was obtained from T. Hasegawa Company.

Yeast suspensions were prepared from 3-d-old yeast colonies. Colonies were removed from the plates and suspended in sterile water, and the optical density at 550 nm of the resulting suspension was measured. The optical density at 550 nm of the suspension was brought to 0.1, serial dilutions (1:10, 1:100, 1:1,000, and 1:10,000) of the suspension were then prepared, and 7 μL of each dilution was spotted on the plates. Plates were grown at 28°C for 3 d.

Synchrotron X-Ray Fluorescence Computed Microtomography

Tomograms were collected at the bending magnet beamline X26A at the National Synchrotron Light Source, Brookhaven National Laboratory. X-ray fluorescence measurements were conducted using a 12-keV monochromatic x-ray beam, which was tuned using a Si(111) channel-cut monochromator. Monochromatic x-rays were focused to a beam size of 5 $\times$ 8 μm using rhodium-coated, silicon Kirkpatrick-Baez microfocusing mirrors. Incident beam energy was monitored using an ion chamber upstream of the focusing optics. X-ray fluorescence spectra were collected with a Vortex-EX silicon-drift detector (SII Nanotechnology) with an active area of 50 mm^2. X-ray transmission through the sample was recorded simultaneously using a p-type, intrinsic, n-type photodiode.

Individual seeds were attached to a 100-μm-diameter silicon fiber using Devcon 5-min epoxy resin, with the micropyle uppermost. The fiber was inserted into a Huber 1001 goniometer, centered, and mounted on a xyzθ stage. During fluorescence microtomography, the seed samples were translated horizontally through the focused x-ray microbeam in step sizes ranging from 5 to 7 μm and then rotated at intervals of between 0.8° to 1.1° angular steps, repeating the translation through a total of 180°. Full-energy dispersive spectra were collected at each pixel with a dwell time of 2 s per pixel. Two-dimensional sinograms (plot of intensity against θ) were computationally reconstructed using fast Fourier transform-based Gridrec software developed by Brookhaven National Laboratory (Dowd et al., 1999), which is controlled by the Interactive Data Language programming software (Research Systems) to provide images of the cross-sectional internal metal distribution.

Elemental abundances (weight fraction) were calculated for the fluorescence measurements, adapted from a description by McNear et al. (2005). Briefly, a thin-film standard reference material (SRM 1833) was measured prior to the collection of each data set to establish sensitivities (counts per s per μg per cm^2) for Fe. We used an assumed object density of 1.2 g cm^{-3} for Arabidopsis seed, a measured voxel size of 3.887 $\times$ 10^{-8} cm^3 (reconstructed pixel area $\times$ beam height), and the average Fe response from the sample to calculate the Fe content of a whole tomogram. This Fe abundance was used as a fixed value for input into the NRLXRF program (Naval Research Laboratory X-Ray Fluorescence; Criss, 1977), from which abundances for potassium, calcium, Mn, nickel, carbon, and Zn were calculated. The concentration precision is typically $\pm$15% and $\pm$10% (1σ) for individual and mean values, respectively.

GFP Fusion Constructs and Intracellular Localization

YSL1 cDNA was amplified by RT-PCR using Platinum Taq DNA Polymerase High Fidelity (Invitrogen) and the following primers: oAtYSL1c.2..27 (5′-CAGTCTCCATGGAAATAGAGCAAAGA-3′) and oAtYSL1c (5′-TCCTCTGAAGCTAAGAACTTCATACAT-3′), which altered the stop codon from TAG to GAG. *YSL1* cDNA was then introduced into the vector psmGFP (CD3-326; Arabidopsis Biological Resource Center) to generate a C-terminal translational fusion to soluble modified GFP (smGFP) under the control of a cauliflower mosaic virus 35S promoter. The 35S::YSL1::GFP fusion construct was then transiently expressed in onion (*Allium cepa*) epidermal cells by biolistic bombardment. For onion bombardment, 6-mg gold microcarriers (1 μm) were coated with 4 μg of DNA in the presence of 50 μL of 2.5 M $CaCl_2$ and 20 μL of 0.1 M spermidine, followed by washing with 70% ethanol and then resuspending in 100% ethanol. Gold microcarriers were placed on the macrocarriers and then bombarded onto onion epidermal peels on 1$\times$ MS medium plates at a distance of 6 cm using the PDS-1000/He instrument (Bio-Rad) with 1,100 p.s.i. helium pressure. The onion epidermal peels were then incubated in the dark at 30°C. After 48 h, samples were mounted in water for microscopic observation.

Full-length *YSL3* genomic DNA was amplified using Platinum Taq DNA Expand High-Fidelity polymerase (Roche) and the following primers: oAtYSL3.26..50 (5′-ACAGTCACATGAACCGGAATCTCGG-3′), and oAtYSL3.4208..4179 (5′-GTAACTCGAATATTTACTCGGCATGAAGCC-3′), which altered the stop codon from TAA to TAC. *YSL3* genomic DNA was then cloned into pDEST-GRuB (pPZP212 backbone with smGFP inserted using *Bam*HI and *Eco*RI sites) to generate a C-terminal translational fusion to smGFP. The YSL3::GFP fusion construct was then stably expressed in *ys1ysl3* double mutant plants following *Agrobacterium tumefaciens*-mediated transformation. Roots of 5-d-old seedlings were mounted in water for microscopic observation. Green fluorescent cells were imaged by a Zeiss 510 Meta Laser Scanning Confocal Microscope (Nikon) with excitation at 488 nm, and the fluorescence emission signal was recovered between 520 and 550 nm.

Inflorescence Grafting

The inflorescences (3–7 cm long, and with similar diameters) of soil-grown Col-0 and *ysl1ysl3* plants were cut using a double-sided blade and then placed in water to prevent drying prior to grafting. A short tube (approximately 0.5–1 cm) of appropriate diameter (Small Parts, Inc.; part no. STT-20-10) was placed over the cut inflorescence stem of the stock, and the tube was filled with distilled water. The scions were then inserted into the other end of the tubing until they touched the stem of the scion. The plants were returned to trays covered with lids for 3 to 5 d to maintain the moisture, allowing plants to recover (Rhee and Somerville, 1995).

Mineral Analysis

Metal ion contents of plant tissues were measured as described (Waters et al., 2006). For soil-grown plants, leaf samples were collected 20 d after sowing.

Quantitative RT-PCR

RNA isolation and RT reactions were performed as described (Waters et al., 2006). Quantitative real-time PCR was performed in a 25-μL reaction volume containing 25 ng (based on the initial input of RNA to the RT reaction) of cDNA, 400 nM each gene-specific primer, and Brilliant II SYBR Green QPCR Master Mix (Stratagene). Primer sequences used were as follows: for Actin2, oAtActin2.qPCR FW (5′-TCTTCCGCTCTTTCTTTCCAAGC-3′) and oAtActin2.qPCR REV (5′-ACCATTGTCACACACGATTGGTTG-3′); for EF-1a, EF-1a.qPCR FW (5′-GCACGCTCTTCTTGCTTTCACC-3′) and EF-1a.qPCR REV (5′-GGGTGGTGGCATCCATCTTGTTAC-3′); and for YSL3, oAtYSL3.qPCR FW (5′-GTTACAGCATTGCAGTTGGAGGTG-3′) and oAtYSL3.qPCR REV (5′-AAGCGGTCATCCAACCGATTCC-3′). The two-step thermal cycling profile used was 15 min at 95°C followed by 40 cycles of 10 s at 95°C and 30 s at 60°C. Following amplification, melt curves were performed to verify that a single product was amplified.

The final threshold cycle (Ct) values were means of three replicates. The comparative $\Delta\Delta$Ct method was used to analyze the results (User Bulletin 2, PRISM sequence detection system; Applied Biosystems). Normalization of the values was based on Actin2 and EF-1a. A negative control with water instead of template was included for each quantitative RT-PCR set.

Overexpression of YSL3

Whole *YSL3* genomic DNA was amplified using Platinum Taq DNA Polymerase High Fidelity (Invitrogen) and the following primers: oAtYSL3.26..50

(5′-ACAGTCACATGAACCGGAATCTCGG-3′) and oAtYSL3.4209..4175 (5′-TTAACTCGAATATTTACTCGGCATGAAGCCCATAC-3′). *YSL3* genomic DNA was cloned into vector pMN20 (Weigel et al., 2000), containing four copies of the cauliflower mosaic virus 35S enhancer. The construct was stably transformed into wild-type Arabidopsis plants, and homozygous transformants were obtained by kanamycin selection.

Chlorophyll Content Determination

For Fe starvation tests, *YSL3* overexpression lines were grown on 1× MS medium for 10 d and then transferred to MS-Fe medium for a variable number of days prior to quantification of chlorophyll. Leaves of soil-grown *YSL3p*::*YSL1* and *YSL3p*::*YSL2* lines were collected at day 20. Shoots and leaves were placed in 1 mL of *N*,*N*′-dimethylformamide, and chlorophyll was extracted overnight. Total chlorophyll was determined as described (Inskeep and Bloom, 1985).

Germination Tests

Seeds were soaked in 0.1% agarose to imbibe at 4°C for 72 h. One hundred seeds were plated onto soil. Percentage viability of seeds was determined 7 d after sowing, at which time germination was scored as successful emergence of the hypocotyls and cotyledons.

Collection and Analysis of Phloem Exudates

Phloem exudates were collected from adult rosette leaves of 25-d-old soil-grown Arabidopsis plants at the start of flowering, using procedures described previously (Fan et al., 2009). The third and fourth leaves were cut, and then the tip of the petiole was recut in EDTA buffer (5 mM Na_2EDTA, pH 7.5, osmotically adjusted to 270 mosmol with sorbitol). Leaves were washed with a large volume of sterile EDTA buffer to remove contaminants and then placed in 200 μL of fresh EDTA buffer. During phloem sap exudation, the leaves were illuminated (25 μE) and incubated at 22°C. After 1 h of bleeding, the buffer solution containing phloem exudates was analyzed for sugar content. Suc and Glc contents were measured by the 3,5-dinitrosalicylic acid method (Bernfeld, 1955).

Complementation of *ysl1ysl3* Double Mutants

The *YSL3* promoter was amplified using Platinum Taq DNA Polymerase High Fidelity (Invitrogen) and the following primers: oAtYSL3.26..50 (5′-ACAGTCACATGAACCGGAATCTCGG-3′) and oAtYSL3.1521..1496 (5′-ACTCCTCAGTTTTTTCCAAGAACAGA-3′). The *YSL3* promoter was then cloned into vector pPZP222. For cloning of *YSL1* and *YSL2* cDNA, a hemagglutinin (HA) tag (YPYDVPDYA) was added to the C terminus of each cDNA in a two-step strategy. *YSL1* cDNA was amplified by RT-PCR using Platinum Taq DNA Polymerase High Fidelity (Invitrogen) and the following primers: oAtYSL1.1526..1555 (5′-CAGTCTCCATGGAAATAGAGCAAAGAAGG-3′) and oAtYSL1.HA1 (5′-GTCGTACGGGTATGAAGCTAAGAACTTCATACATATCGGAGG-3′), which altered the stop codon from TAG to TAC and added the first 12 nucleotides of the HA tag to the 3′ end of the *YSL1* cDNA. A secondary PCR was then performed using primary PCR product as template and the following primers: oAtYSL1.1526..1555 (5′-CAGTCTCCATGGAAATAGAGCAAAGAAGG-3′) and oAtYSL1.HA2 (5′-TCACGCGTAGTCCGGCACGTCGTACGGGTATGAAGCTAAGAACTT-3′), which added the entire HA tag sequence to the 3′ end of the *YSL1* cDNA. *YSL2* cDNA was amplified using the same method as for *YSL1* cDNA. Primers for *YSL2* primary PCR were oAtYSL2.1541..1567 (5′-CTTCAAATGGAAAACGAAAGGGTTGAG-3′) and oAtYSL2.HA1 (5′-GTCGTACGGGTAATGAGCCGCAGTGAAGTTCATACAGATA-3′). Primers for *YSL2* secondary PCR were oAtYSL2.1541..1567 (5′-CTTCAAATGGAAAACGAAAGGGTTGAG-3′) and oAtYSL2.HA2 (5′-TCACGCGTAGTCCGGCACGTCGTACGGGTAATGAGCCGCAGT-3′). *YSL1* and *YSL2* cDNA were cloned into the vector YSL3p/pPZP222 under the control of the *YSL3* promoter. *YSL3p*::*YSL1* and *YSL3p*::*YSL2* constructs were then stably transformed into the *ysl1ysl3* double mutant and selected using gentamycin resistance.

Supplemental Data

The following materials are available in the online version of this article.

Supplemental Figure S1. The sequence of the protein encoded by the *AtYSL3* cDNA.

Supplemental Figure S2. Synchrotron x-ray fluorescence computed microtomography showing the distribution and abundance (in $\mu g\ g^{-1}$) of Mn, Cu, and Zn.

ACKNOWLEDGMENTS

We gratefully thank Teddi Bloniarz for her expert assistance with growth chambers and in the greenhouse, David Eide for providing us with helpful advice and with yeast strains, and Mary Lou Guerinot for critical reading of the manuscript.

Received May 11, 2010; accepted July 12, 2010; published July 12, 2010.

LITERATURE CITED

Anderegg G, Ripperger H (1989) Correlation between metal complex formation and biological activity of nicotianamine analogues. J Chem Soc Chem Commun **10:** 647–650

Bernfeld P (1955) Amylases, alpha and beta. Methods Enzymol **1:** 149–158

Criss JW (1977) NRLXRF, A FORTRAN Program for X-Ray Fluorescence Analysis. Naval Research Laboratory, Washington, DC

Curie C, Cassin G, Couch D, Divol F, Higuchi K, Le Jean M, Misson J, Schikora A, Czernic P, Mari S (2009) Metal movement within the plant: contribution of nicotianamine and yellow stripe 1-like transporters. Ann Bot (Lond) **103:** 1–11

Curie C, Panaviene Z, Loulergue C, Dellaporta SL, Briat JF, Walker EL (2001) Maize *yellow stripe1* encodes a membrane protein directly involved in Fe(III) uptake. Nature **409:** 346–349

DiDonato RJ Jr, Roberts LA, Sanderson T, Eisley RB, Walker EL (2004) Arabidopsis Yellow Stripe-Like2 (YSL2): a metal-regulated gene encoding a plasma membrane transporter of nicotianamine-metal complexes. Plant J **39:** 403–414

Dowd BA, Campbell GH, Marr RB, Nagarkar VV, Tipnis SVLA, Siddons DP (1999) Developments in synchrotron x-ray computed microtomography at the National Synchrotron Light Source. Proc SPIE **3772:** 224–236

Fan SC, Lin CS, Hsu PK, Lin SH, Tsay YF (2009) The *Arabidopsis* nitrate transporter NRT1.7, expressed in phloem, is responsible for source-to-sink remobilization of nitrate. Plant Cell **21:** 2750–2761

Gao CY, Pinkham JL (2000) Tightly regulated, beta-estradiol dose-dependent expression system for yeast. Biotechniques **29:** 1226–1231

Gendre D, Czernic P, Conejero G, Pianelli K, Briat JF, Lebrun M, Mari S (2007) TcYSL3, a member of the YSL gene family from the hyperaccumulator Thlaspi caerulescens, encodes a nicotianamine-Ni/Fe transporter. Plant J **49:** 1–15

Grusak MA (1994) Iron transport to developing ovules of *Pisum sativum*. 1. Seed import characteristics and phloem iron-loading capacity of source regions. Plant Physiol **104:** 649–655

Guerinot ML, Yi Y (1994) Iron: nutritious, noxious, and not readily available. Plant Physiol **104:** 815–820

Herbik A, Koch G, Mock HP, Dushkov D, Czihal A, Thielmann J, Stephan UW, Baumlein H (1999) Isolation, characterization and cDNA cloning of nicotianamine synthase from barley: a key enzyme for iron homeostasis in plants. Eur J Biochem **265:** 231–239

Higuchi K, Suzuki K, Nakanishi H, Yamaguchi H, Nishizawa NK, Mori S (1999) Cloning of nicotianamine synthase genes, novel genes involved in the biosynthesis of phytosiderophores. Plant Physiol **119:** 471–480

Himelblau E, Amasino RM (2001) Nutrients mobilized from leaves of Arabidopsis thaliana during leaf senescence. J Plant Physiol **158:** 1317–1323

Hocking PJ, Pate JS (1977) Mobilization of minerals to developing seeds of legumes. Ann Bot (Lond) **41:** 1259–1278

Hocking PJ, Pate JS (1978) Accumulation and distribution of mineral elements in annual lupins Lupinus albus L and Lupinus angustifolius L. Aust J Agric Res **29:** 267–280

Inoue H, Kobayashi T, Nozoye T, Takahashi M, Kakei Y, Suzuki K, Nakazono M, Nakanishi H, Mori S, Nishizawa NK (2009) Rice OsYSL15 is an iron-regulated iron(III)-deoxymugineic acid transporter expressed in the roots and is essential for iron uptake in early growth of the seedlings. J Biol Chem **284:** 3470–3479

Inskeep WP, Bloom PR (1985) Extinction coefficients of chlorophyll a and b in *N*,*N*-dimethylformamide and 80% acetone. Plant Physiol **77:** 483–485

Kim SA, Punshon T, Lanzirotti A, Li L, Alonso JM, Ecker JR, Kaplan J, Guerinot ML (2006) Localization of iron in Arabidopsis seed requires the vacuolar membrane transporter VIT1. Science **314:** 1295–1298

Klatte M, Schuler M, Wirtz M, Fink-Straube C, Hell R, Bauer P (2009) The analysis of Arabidopsis nicotianamine synthase mutants reveals functions for nicotianamine in seed iron loading and iron deficiency responses. Plant Physiol **150:** 257–271

Koike S, Inoue H, Mizuno D, Takahashi M, Nakanishi H, Mori S, Nishizawa NK (2004) OsYSL2 is a rice metal-nicotianamine transporter that is regulated by iron and expressed in the phloem. Plant J **39:** 415–424

Lee S, Chiecko JC, Kim SA, Walker EL, Lee Y, Guerinot ML, An G (2009) Disruption of OsYSL15 leads to iron inefficiency in rice plants. Plant Physiol **150:** 786–800

Le Jean M, Schikora A, Mari S, Briat JF, Curie C (2005) A loss-of-function mutation in AtYSL1 reveals its role in iron and nicotianamine seed loading. Plant J **44:** 769–782

Ling HQ, Koch G, Baumlein H, Ganal MW (1999) Map-based cloning of chloronerva, a gene involved in iron uptake of higher plants encoding nicotianamine synthase. Proc Natl Acad Sci USA **96:** 7098–7103

McNear D, Peltier E, Everhart J, Chaney R, Sutton S, Newville M, Sparks DL (2005) Application of quantitative fluorescence and absorption-edge computed microtomography to image metal compartmentalization in Alyssum murale. Environ Sci Technol **39:** 2210–2218

Mora-Garcia S, Vert G, Yin Y, Cano-Delgado A, Cheong H, Chory J (2004) Nuclear protein phosphatases with Kelch-repeat domains modulate the response to brassinosteroids in Arabidopsis. Genes Dev **18:** 448–460

Murata Y, Ma JF, Yamaji N, Ueno D, Nomoto K, Iwashita T (2006) A specific transporter for iron(III)-phytosiderophore in barley roots. Plant J **46:** 563–572

Oldenburg KR, Vo KT, Michaelis S, Paddon C (1997) Recombination-mediated PCR-directed plasmid construction in vivo in yeast. Nucleic Acids Res **25:** 451–452

Pich A, Scholz G (1996) Translocation of copper and other micronutrients in tomato plants (Lycopersicon esculentum Mill.): nicotianamine-stimulated copper transport in the xylem. J Exp Bot **47:** 41–47

Rhee SY, Somerville CR (1995) Flat-surface grafting in Arabidopsis thaliana. Plant Mol Biol Rep **13:** 118–123

Roberts LA, Pierson AJ, Panaviene Z, Walker EL (2004) Yellow stripe1: expanded roles for the maize iron-phytosiderophore transporter. Plant Physiol **135:** 112–120

Romheld V, Marchner H (1986) Evidence for a specific uptake system for iron phytosiderophores in roots of grasses. Plant Physiol **80:** 175–180

Schaaf G, Ludewig U, Erenoglu BE, Mori S, Kitahara T, von Wirén N (2004) ZmYS1 functions as a proton-coupled symporter for phytosiderophore- and nicotianamine-chelated metals. J Biol Chem **279:** 9091–9096

Schaaf G, Schikora A, Haberle J, Vert G, Ludewig U, Briat JF, Curie C, von Wiren N (2005) A putative function for the Arabidopsis Fe-phytosiderophore transporter homolog AtYSL2 in Fe and Zn homeostasis. Plant Cell Physiol **46:** 762–774

Schmidke I, Stephan UW (1995) Transport of metal micronutrients in the phloem of castor bean (*Ricinus communis*) seedlings. Physiol Plant **95:** 147–153

Stephan UW, Scholz G, Rudolph A (1990) Distribution of nicotianamine, a presumed symplast iron transporter, in different organs of sunflower and of a tomato wild type and its mutant chloronerva. Biochem Physiol Pflanz **186:** 81–88

Tagaki S, Nomoto K, Takemoto T (1984) Physiological aspect of mugineic acid, a possible phytosiderophore of graminaceous plants. J Plant Nutr **7:** 469–477

Takahashi M, Terada Y, Nakai I, Nakanishi H, Yoshimura E, Mori S, Nishizawa NK (2003) Role of nicotianamine in the intracellular delivery of metals and plant reproductive development. Plant Cell **15:** 1263–1280

Tian GW, Mohanty A, Chary SN, Li S, Paap B, Drakakaki G, Kopec CD, Li J, Ehrhardt D, Jackson D, et al (2004) High-throughput fluorescent tagging of full-length Arabidopsis gene products in planta. Plant Physiol **135:** 25–38

von Wiren N, Klair S, Bansal S, Briat JF, Khodr H, Shioiri T, Leigh RA, Hider RC (1999) Nicotianamine chelates both Fe[III] and Fe[II]: implications for metal transport in plants. Plant Physiol **119:** 1107–1114

Waters BM, Chu HH, Didonato RJ, Roberts LA, Eisley RB, Lahner B, Salt DE, Walker EL (2006) Mutations in Arabidopsis *Yellow Stripe-Like1* and *Yellow Stripe-Like3* reveal their roles in metal ion homeostasis and loading of metal ions in seeds. Plant Physiol **141:** 1446–1458

Waters BM, Grusak MA (2008) Whole-plant mineral partitioning throughout the life cycle in Arabidopsis thaliana ecotypes Columbia, Landsberg erecta, Cape Verde Islands, and the mutant line ysl1ysl3. New Phytol **177:** 389–405

Weigel D, Ahn JH, Blazquez MA, Borevitz JO, Christensen SK, Fankhauser C, Ferrandiz C, Kardailsky I, Malancharuvil EJ, Neff MM, et al (2000) Activation tagging in Arabidopsis. Plant Physiol **122:** 1003–1013